Available online at www.sciencedirect.com

ScienceDirect

Procedia Structural Integrity 2 (2016) 2156–2163

Structural Integrity Procedia

www.elsevier.com/locate/procedia

21st European Conference on Fracture, ECF21, 20-24 June 2016, Catania, Italy

Fatigue life prediction of high strength steel welded joints by Energy Approach

P. Corigliano, V. Crupi, G. Epasto, E. Guglielmino, G. Risitano*

Department of Engineering, University of Messina, Contrada Di Dio (S. Agata), 98166 Messina, Italy

Abstract

Two full-field techniques were applied for the study of the base material and welded specimens, made of S690QL steel: digital image correlation and thermographic techniques. Static and fatigue tests were carried out. The thermographic measurements can be used to predict the fatigue, with a great saving in time and effort. Fatigue tests at increasing loads were carried out by a stepwise succession, applied to the same specimen, for applying an energy-based approach. The predictions of the fatigue life, obtained by means of the Energy Approach, were compared with the values obtained by the traditional procedure.

Keywords: Thermographic Method; Energy Approach; Fatigue; S-N curve; Welded joints; High strength steel; Digital Image Correlation; Infrared Thermography

1. Introduction

The infrared thermography was applied for the analysis of different materials under fatigue loading: short glass fiber-reinforced polyamide composites by Crupi et al. (2015), shape memory alloys by Maletta et al. (2014), and steels in low cycle fatigue (LCF) regime by Corigliano et al. (2015), high cycle fatigue (HCF) regime [Risitano et al. (2015), Amiri et al. (2010), Wang et al. (2012), Meneghetti et al. (2015), Curà et al. (2005), De Finis et al. (2015)] and very high cycle fatigue (VHCF) regime by Plekhov et al. (2015) and Crupi et al. (2015). The fatigue effects become even more important in presence of welded joints and the fatigue assessment of welded joints becomes more complex in presence of a multiaxial stress state as demonstrated by Susmel (2014). The literature on fatigue analysis

* Corresponding author. Tel.: +39 347 3209239.
E-mail address: giacomo.risitano@unime.it

10.1016/j.prostr.2016.06.270

of welded joints was reviewed by Fricke (2015). The Thermographic Method (TM) was already applied for the fatigue assessment of welded joints by Crupi et al. (2007), Fan et al. (2011), Williams et al. (2013).

The aim of this study is the application of an energy-based approach for the fatigue assessment of base material and welded joints, made of S690QL steel. Tensile and fatigue tests were carried out. Digital Image Correlation (DIC) and infrared thermography techniques (IRT) have been used during static tests. IR camera was used for detecting the temperature during the fatigue tests in order to apply an energy-based approach. The predictions of the fatigue limit were compared with the values obtained applying the traditional procedure.

2. Material and methods

A commercial high strength structural steel (HSSS), with a thickness of 5 mm is tested in quenched and tempered condition (Q + T) corresponding to European Standard Steel EN 10137-2 S690QL. In this study, base material and butt welded -joint specimens were investigated. The chemical composition of the steel is given in Table 1. The carbon content of the quenched and tempered high strength steels is generally small, and the main alloying elements are Mn, Mo, Cr, Ni and micro-alloying element, as Ti.

The geometry of the investigated specimens is shown in Fig. 1. The static tensile tests were carried out on base material specimens and butt-welded specimens with welds overfill removed, using a servo-hydraulic load machine (INSTRON 8854) at a crosshead rate equal to 3 mm/min on base material and welded specimens. The DIC and IR camera have been used during all tests (Fig. 2). ARAMIS 3D 12M system was used to analyze the strain pattern of the specimen surface. Two cameras with a resolution of 4000 x 3000 pixels, with a focal length of 50 mm, were used. The system accuracy for the strain measurement is up to 0.01%, while the highest acquisition frequency is 58 Hz at max resolution. The temperature evolution during the static tests was analysed by a 1280 × 1024 pixels InSb focal plane array cooled detector infrared camera (model FLIR Systems SC 8400), working in the MWIR (1.5–5.1 μm) spectral band (NETD 20 mK at 30 °C). A 100 mm focal length lens (FOV 11° × 9° and equipped with a 18 mm extension ring) was used. The thermographic images were acquired at 90 fps by FLIR ResearchIR software, in sub-windowing resolution, at 216 × 228 pixels. The specimens were coated with black paint and the IR camera was placed on the opposite side of the specimen respect to the DIC equipment (Fig. 1).

Fatigue tests were carried out at R = 0.1 and f = 10 Hz by the same servo-hydraulic load machine (INSTRON 8854). Constant amplitude values of the stress range till failure were applied and, according to the TM, tests at increasing loads were carried out by a stepwise succession (applied to the same specimen). The specimens have the same geometry (Fig. 1) of those used for the static tests and are made from the same steel. In order to apply the TM, the specimens were coated with black paint and the temperature increment of the specimen surface was detected during the fatigue tests by an IR camera (model FLIR Systems SC640), an uncooled long wave infrared (LWIR) focal plane array camera with a resolution of 640x480 pixels and a measurement accuracy of ±2 °C. The frame rate during the acquisition of thermal increment was 30 fps in the first stage until temperature plateau was reached; then the frame rate was changed to 1 frame per minute.

Table 1. Chemical composition of EN 10137-S690QL (in wt. %).

Si	Mn	P	S	Cr	Mo	Ni	Al	Co	Nb	Ti	V	W	Pb	Sn	Cd	Fe
0,71	0,92	0.050	0,16	0,33	0.19	0.14	0.66	0.19	0,031	0.052	0.020	0.093	0.050	0.051	0.054	**balance**

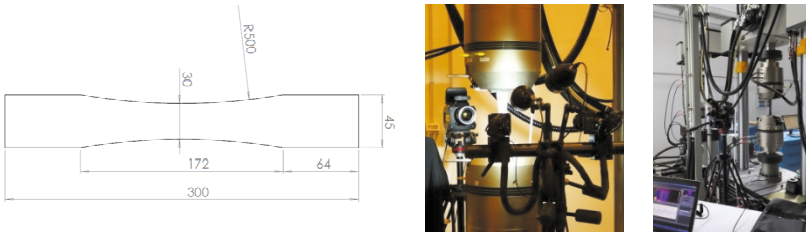

(a) (b) (c)

Fig. 1. (a) specimen geometry; (b) and (c) experimental setup.

3. Results and discussion

3.1. Static tests

Fig. 2 shows the strain contour at different test steps of a base material specimen and reveals the strain localizations, accompanying band nucleation, in the middle of specimen length when yield load is reached (35 s). The nucleation of a second band, giving a X-shape pattern, can be seen at increasing loads. Strain localization bands were observed during static tests, also for welded joints (Fig. 2). A first band was detected at yielding, including the weld, then the weld acted as more rigid material dividing the first band and obtaining two separate bands around 815 MPa. By increasing the stress level, the nucleation of a second band, giving a X-shape pattern, can be seen for each of the two bands. At even higher stresses the second band is the one that brings the specimen to fracture.

Fig. 3 shows the stress-strain curve of a welded specimen for points at different distance of the weld in order to detect the behaviour of the different zones (BM, HAZ, WM). It is possible to see that, at a stress level equal to 750 MPa (prior to yielding) the weld toe has a higher level of strains with respect to points of the base material, showing no significant differences with respect to non-welded specimens as the specimen shows its higher strain in correspondence of its middle position. A considerable difference is depicted in the plastic phase, i.e. at 852 MPa, where the weld shows a strain level more or less equal to 1,5 %, while at a distance of 5 mm the strain is almost of 2,4 % and at a distance of 10 and 15 mm the strain is considerably higher. This behaviour is confirmed also by Fig. 4, which shows the strain- distance from the weld-center curve and the HV hardness-distance from weld-center curve. In particular the maximum strain is detected at a distance of 10 mm, where a high drop of hardness is measured.

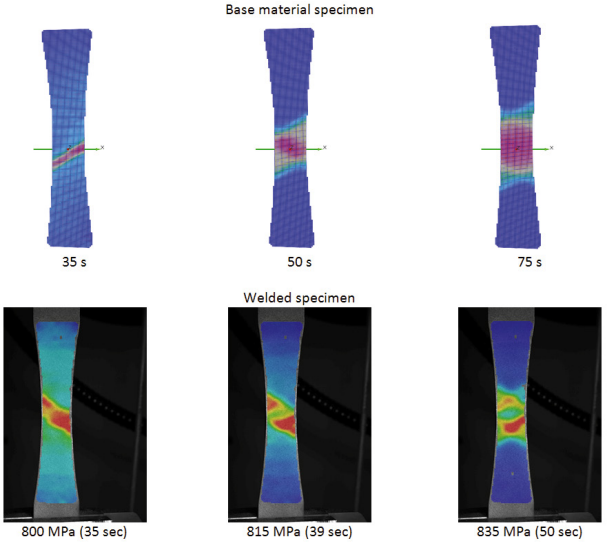

Fig. 2. Strain pattern of a base material specimen and a welded specimen during static test

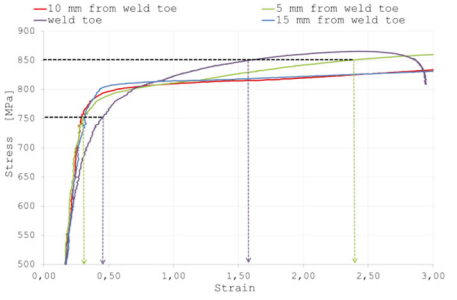

Fig. 3. Stress-strain curve of a welded specimen for points at different distance from weld.

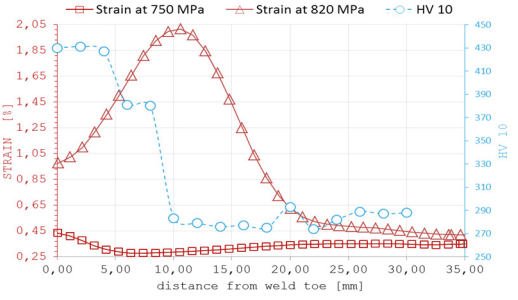

Fig. 4. Strain-distance from weld-center curve and HV hardness-distance from weld-center curve.

3.2 Fatigue tests

The temperature of the specimen surface was detected by an IR camera during each fatigue test. The ΔT – N curve, obtained during the fatigue test, shows the typical three phases of TM, as displayed in Fig. 5: a rapid increment in phase I, an almost constant value during phase II, and a sudden increase in phase III just before the specimen failure.

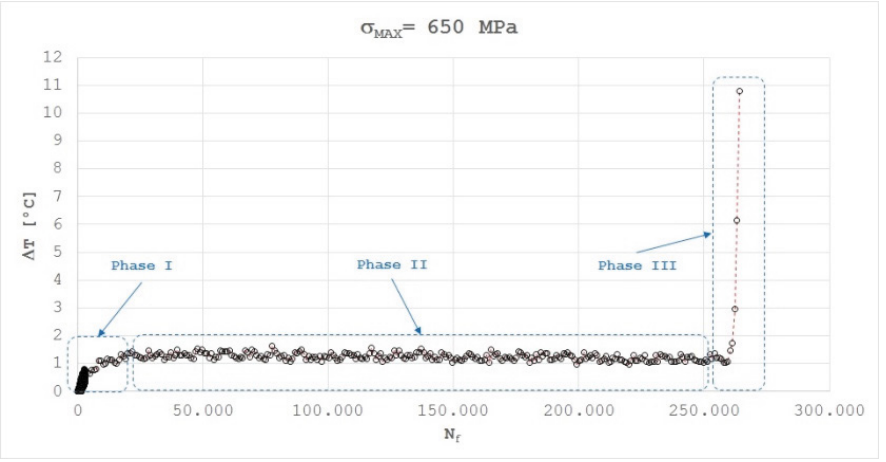

Fig. 5. ΔT – N curve.

The TM allows the prediction of the fatigue life and the rapid determination of the entire S–N curve by means of an energy-based approach. The basic assumption of the ‘‘Energy Approach’’ is that the fatigue failure takes place when the absorbed energy reaches a certain threshold value E_C characteristic for each structural detail. The limit energy E_C is proportional to the integral Φ of the ΔT – N curve. Considering that the number of cycles of the phases I and III is negligible compared with that of phase II, the integral Φ can be practically assumed equal to the product of temperature increment during the phase II to the fatigue number of cycles ($\Phi \approx \Delta T_{AS} \bullet N_f$). Thus, it is possible to obtain the fatigue number of cycles by the knowledge of the integral Φ and the temperature increment ΔT_{AS} at each applied stress range level Δσ.

The values of fatigue life predicted by the ‘‘Energy Approach’’ are close to the experimental values obtained by constant amplitude fatigue tests as shown in Fig. 6. The welded specimens exhibit some scatter probably due to welding imperfections as reported in section 3.3. The fatigue tests allows to estimate the fatigue limit, assumed as the higher value of maximum stress which doesn't produce the failure after $5 \bullet 10^6$ cycles: $\sigma_{0max} \approx 530$ MPa for base material specimens, $\sigma_{0max} \approx 300$ MPa for welded specimens,.

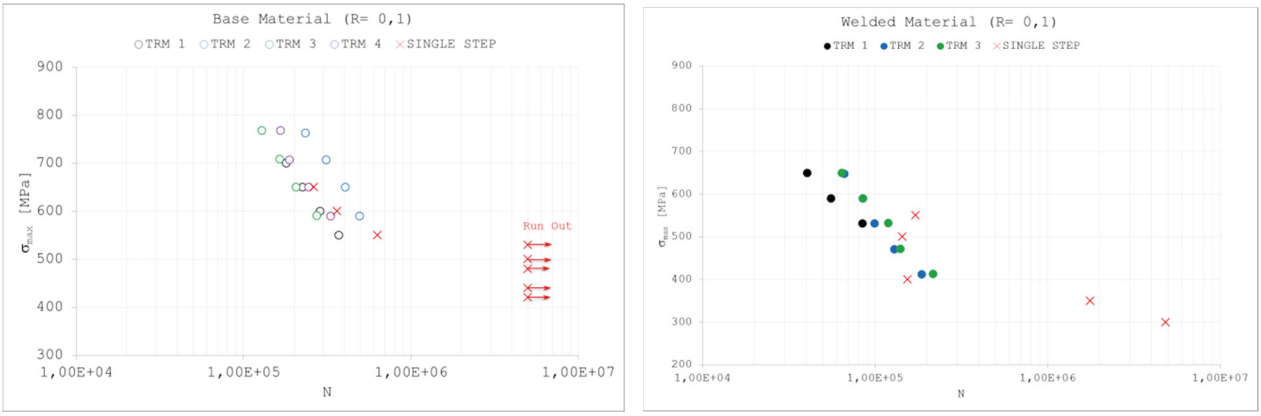

(a) (b)

Fig. 6. Fatigue life obtained by Energy Approach and fatigue tests: (a) base material specimens; (b) welded specimens.

3.3 Fracture analysis

Welded joints are susceptible to material discontinuities and defects (such as porosity, slag inclusions, hot and cold cracks, lack of fusion, incomplete penetration) and can also cause undesirable strength mismatch [Zerbst et al. (2014)], resulting in the hardening effects shown in Fig. 4. Due to hardening effect, the mechanical strength can locally increase. This behavior is related to the generation of a martensite or bainite, which are usually undesired because of their deleterious effect on fatigue strength. Because of the inhomogeneous microstructure of the weld joint, the fracture toughness shows a significant scatter depending on the crack tip position along the welded joint. If the crack does not immediately stops for a local microstructural barrier, the crack propagates, deviates into the lower strength and, probably, higher toughness area. In S690QL steel, this will cause ductile morphology of the fracture surface in the stable propagation area, even though some differences can be found between LCF and HCF regime. The crack path deviation is shown in Fig. 7a. The crack path deviation is just due to the welding and it was not detected in the base material specimen tested in the same experimental conditions (Fig. 7b). Pores can be also found in the fracture surface and are attributed to the weld process. The crack propagation per cycle is very rapid, resulting in a LCF surface fracture (Fig. 7a).

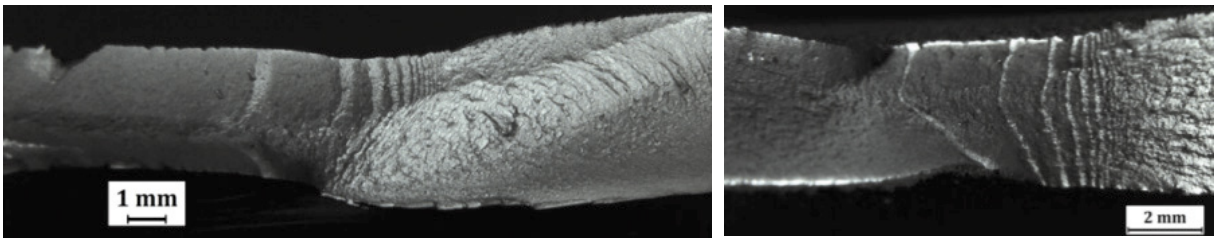

Fig. 7. Fatigue fracture surfaces of (a) welded and (b) base material (σ_{max}=550 MPa).

By means of scanning electron microscope (SEM), the microscopic growth process is shown in Fig. 8 with the presence of dimples and fatigue striations. It should be noted that the specimen is relatively thin, and that fatigue growth can be assumed to be under plane-stress conditions [Lampman (1998)]. This contributes to the formation of shear dimples, oriented along shear direction.

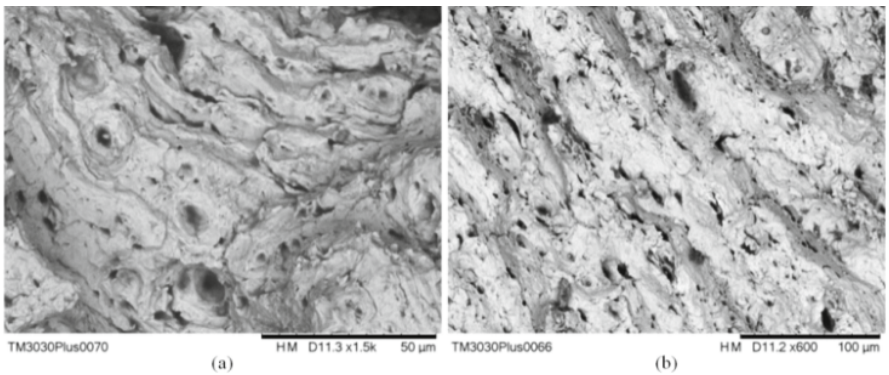

Fig. 8. (a) SEM fatigue fracture surface showing stable crack propagation region of HAZ of welded specimen; (b) fatigue striations.

The porosity (Fig. 9), porosity clusters (Fig. 10d) and the inclusions (Fig. 10b) detected on the fracture surfaces seem to not affect the mechanical response of the tested steel.
Indeed, non-destructive defect evaluation of the joints was carried out before testing (Fig. 9) and keep in account in the planning of the fatigue tests.
As found on the fracture surface, in HAZ (Fig. 10a) the welding process can also induce inclusions rich in iron (Fig. 10b), as shown in the EDS spectrum (Fig. 10c).

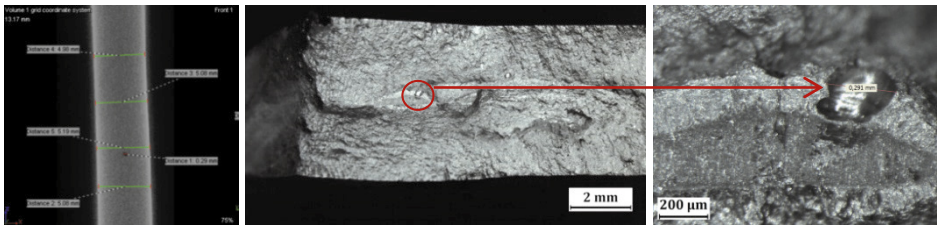

Fig. 9. Fatigue fracture surface of a welded specimen (σ_{max}=500 MPa).

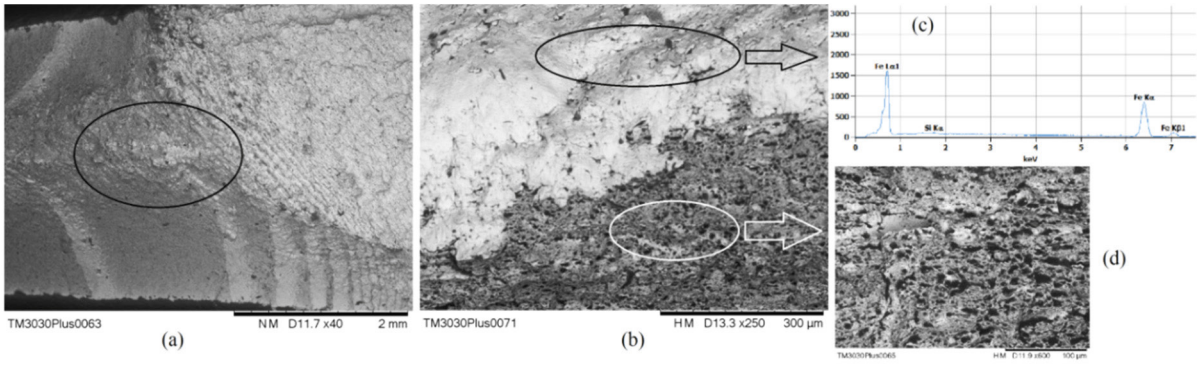

Fig. 10. SEM fatigue fracture surface for (a) HAZ of the joint; (b) rich in iron zone; (c) EDS spectrum; (d) porosity clusters.

The fibrous zone on the fracture surface of the welded specimen subjected to static tensile test is not so evident, while radial and shear lips are easily detectable (Fig. 11, at different magnifications). The EDS spectrum (Fig. 11d) shows no appreciable difference in the chemical composition in the area in which high plastic deformation can be found (Fig. 11a).

The analysis of the static loaded welded specimen allows the understanding of the tensile failure for the studied geometry. The elongation is governed by strain instability, which leads to neck formation followed to the appearing of surface bands for the non-welded specimens of the same steel. By means of DIC and IRT, a similar behavior is observed also on the welded joint. Being the specimen flat, two kinds of neck can be seen of its surfaces: maybe, the first is a diffuse neck and the second a local neck. The diffuse neck forms firstly and involves the whole gauge length. The local neck is associated to the appearing of the bands near the site in which crack initiated. By IR and DIC analysis, the angle of the band is measured to be about 36°C (x-axes for DIC). The necking results in an X-shape fracture on the through thickness face (Fig. 11e).

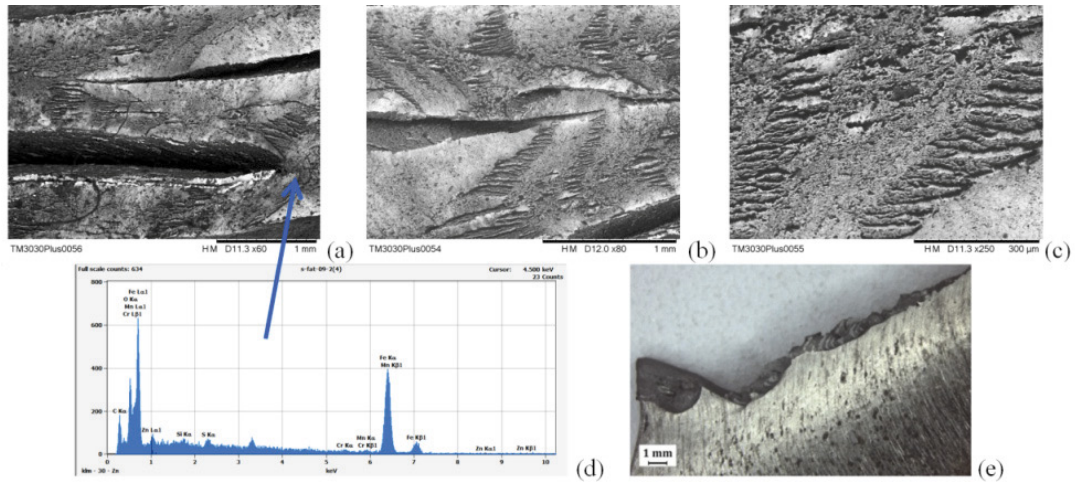

Fig. 11. Static tensile test of a welded specimen fracture surface: (a), (b) and (c) SEM fracture surface; (e) through thickness fracture surface.

The load value involving local necking and Lüders band detection is found to be in the interval of 35–47 s. The thermograms plotting the thermal response due to the nucleation and propagation of the bands are reported in Fig. 12. At 35 s, temperature increment localizes at the toe of the welding, maybe due to a local stress concentration induced by the welding itself, even though the seam has been smoothed (Fig. 12a) or by the strength mismatch. The temperature plot referred to the ROI 3 shows that in the site of band nucleation, ΔT is about 0.4°C respect to the opposite region (ROI 1). ROI 2 includes welding seam which is apparently no involved in the band propagation. The second band appears at 38 s, overlaps the first one and gives an X-shape thermal image; in the meantime, a new band appears at the top toe of the welding (Fig. 12b). At 47 s, some crack starts appearing. The thermograms in Fig. 12a, b and c were processed by means of a window average filter (3x3 kernel) in order to enhance thermal details.

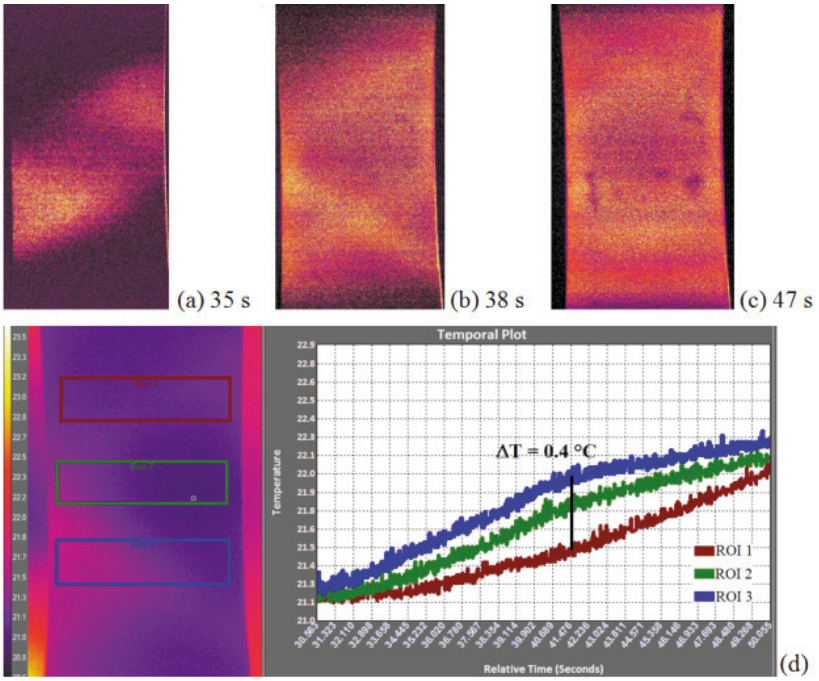

Fig. 12. Temperature pattern accompanying Lüders band nucleation at different time steps (a), (b) and (c); (d) Temperature plot for the unfiltered thermograms sequence in the selected ROIs

4. Conclusions

Full-field techniques were applied for the study of S690QL base material and welded specimens. The DIC technique allowed the detection of strain localizations in base material specimens, accompanying band nucleation, in the middle of specimen length when yield load is reached. The same technique applied to welded specimens showed the different behaviour of the three zones (BM, HAZ, WM) during static tests, revealing higher localization of strains in the WM with respect to HAZ and BM, for a lower level of stress than the yield stress. A higher level of strain is detected in the HAZ and in the BM, in the plastic field, where a drop in hardness is detected, causing the specimen failure.

The IRT technique was also applied during static tests confirming the DIC results and fatigue tests. The Thermographic Method allows the prediction of the fatigue life of base material specimens and welded specimens. By means of an energy approach. The predicted values are in good agreement with the experimental values of fatigue life.

For fatigued specimens, tested in the same experimental conditions, by the microscopic evaluation of the fracture surfaces, a crack path deviation, due to the welding and not detected in the base material, can be seen. The welding defects, detected on the fracture surfaces, seem to not affect the mechanical response of the tested steel.

The results gave interesting information for the development of prediction models for the fatigue life assessments of welded joints made of HSSS with overfill removed.

Acknowledgements

The research reported in this paper was conducted with the financial support of the Research Project STEM-STELO, ("Systems and technologies for the realization of machinery in order to develop exceptional Transportation and project logistic"), funded by the PON (National Operative Programme) 2007-2013, and with the facilities of the Research Project "CERISI" ("Research and Innovation Centre of Excellence for Structure and Infrastructure of large dimensions"), funded by the PON (National Operative Programme) 2007-2013.

References

Amiri M., Khonsari M.M., 2010. Rapid determination of fatigue failure based on temperature evolution: Fully reversed bending load. International Journal of Fatigue 32, 382–389.

Corigliano P., Crupi V., Fricke W., Friedrich N., Guglielmino E., 2015. Experimental and numerical analysis of fillet-welded joints under low-cycle fatigue loading by means of full-field techniques. Special Issue "Fatigue Design and Analysis in Transportation Engineering", Proceedings of the Institution of Mechanical Engineers, Part C: Journal of Mechanical Engineering Science 229, 1327-1338.

Curà F., Curti G., Sesana R., 2005. A new iteration method for the thermographic determination of fatigue limit in steels, International Journal of Fatigue 27, 453–459.

Crupi V., Guglielmino E., Risitano G., Tavilla F., 2015. Experimental analyses of SFRP material under static and fatigue loading by means of thermographic and DIC techniques. Composites Part B: Engineering 77, 268-277.

Crupi V., Epasto G., Guglielmino E., Risitano G., 2015. Thermographic method for very high cycle fatigue design in transportation engineering, Special Issue "Fatigue Design and Analysis in Transportation Engineering", Proceedings of the Institution of Mechanical Engineers Part C: Journal of Mechanical Engineering Science 229, 1260-1270.

Crupi V., Epasto G., Guglielmino E., Risitano G., 2015. Analysis of temperature and fracture surface of AISI4140 steel in very high cycle fatigue regime. Theoretical and Applied Fracture Mechanics 80, 22-30.

Crupi V., Guglielmino E., Risitano A., Taylor D., 2007. Different methods for fatigue assessment of T welded joints used in ship structures. Journal of Ship Research 51, 150-159.

De Finis R., Palumbo D., Ancona F., Galietti U., 2015. Fatigue limit evaluation of various martensitic stainless steels with new robust thermographic data analysis. International Journal of Fatigue 74, 88-96.

Fan J.L., Guo X.L., Wu C.W., Zhao Y.G., 2011. Research on fatigue behavior evaluation and fatigue fracture mechanisms of cruciform welded joints, Materials Science and Engineering: A 528, 8417-8427.

Fricke W., 2015. Recent Developments and Future Challenges in Fatigue Strength Assessment of Welded Joints. Special Issue "Fatigue Design and Analysis in Transportation Engineering", Proceedings of the Institution of Mechanical Engineers, Part C: Journal of Mechanical Engineering Science 229, 1234-1249.

Maletta C., Bruno L., Corigliano P., Crupi V., Guglielmino E., 2014.Crack-tip thermal and mechanical hysteresis in Shape Memory Alloys under fatigue loading. Materials Science and Engineering: A, Structural Materials: Properties, Microstructure and Processing 616, 281–287.

Meneghetti G., Ricotta M., Atzori B., 2015. Experimental evaluation of fatigue damage in two-stage loading tests based on the energy dissipation. Proceedings of the Institution of Mechanical Engineers, Part C: Journal of Mechanical Engineering Science 229, 1280-1291.

Plekhov O., Naimark O., Semenova I., Polyakov A., Valiev R., 2015. Experimental study of thermodynamic and fatigue properties of submicrocrystalline titanium under high cyclic and gigacyclic fatigue regime. Special Issue "Fatigue Design and Analysis in Transportation Engineering", Proceedings of the Institution of Mechanical Engineers, Part C: Journal of Mechanical Engineering Science 229, 1271-1279.

Risitano A., La Rosa G., Geraci A., Guglielmino E., 2015. The choice of thermal analysis to evaluate the monoaxial fatigue strength on materials and mechanical components. Special Issue "Fatigue Design and Analysis in Transportation Engineering", Proceedings of the Institution of Mechanical Engineers, Part C: Journal of Mechanical Engineering Science 229, 1315-1326.

Steven, R. Lampman, 1998. ASM Handbook: Volume 19: Fatigue and Fracture.

Susmel L., 2014. Nominal stresses and Modified Wöhler Curve Method to perform the fatigue assessment of uniaxially loaded inclined welds. Proceedings of the Institution of Mechanical Engineers, Part C: Journal of Mechanical Engineering Science 228, 2871–2880.

Zerbst U., R.A. Ainsworth, H.T.H. Beier, et al., 2014. Review on fracture and crack propagation in weldments– Afracture mechanics perspective. Engineering Fracture Mechanics 132 (2014): 200-276.

Wang X.G., Crupi V., Guo X.L., Guglielmino E., 2012. A thermography-based approach for structural analysis and fatigue evaluation. Proceedings of the Institution of Mechanical Engineers, Part C: Journal of Mechanical Engineering Science 26, 1173-1185.

Williams P., Liakat M.., Khonsari M.M., Kabir O.M., 2013. A thermographic method for remaining fatigue life prediction of welded joints. Materials & Design 51, 916-923.